Shaper Design in CMOS for High Dynamic Range

Gianluigi De Geronimo and Shaorui Li

***Abstract*—We start with an analysis of the configurations commonly adopted to implement linear shapers. We show that, once the ENC from the charge amplifier is defined, the dynamic range of the system is set by the voltage swing and the value of the capacitance realizing the poles. The configuration used to realize the poles has also an impact, and those configurations based on passive components in feedback are expected to offer a higher dynamic range than the ones that use both active and passive components, like scaling mirrors. Finally, we introduce the concept of delayed dissipative feedback (DDF), which consists of delaying the resistive feedbacks from the furthest available nodes along the shaping chain. We will show that, in order to implement semi-Gaussian shapers, a small capacitor in positive feedback is required. The DDF technique can overcome some of the limitations of the more classical configurations. For example, in a third order shaper a factor of two higher dynamic range can be obtained or, at equal dynamic range, about 25% of the capacitance is needed (i.e. about 30% of the area in practical cases).**

***Index Terms*—CMOS, high dynamic range, low-noise, shaper.**

I. Introduction

FRONT-END electronics for capacitive sensors typically includes a preamplifier followed by a filter. The preamplifier provides low-noise amplification of the signals induced in the sensor electrodes. The filter, by properly limiting the signal bandwidth, maximizes the signal-to-noise (S/N) ratio. Additionally the filter limits the duration of the output signal associated with the measured event and, for those sensors where the induced signal is relatively slow, it maximizes the signal amplitude (i.e. it minimizes the ballistic deficit) [1].

Filters can be either time-variant or time-invariant. In electronics for radiation sensors, filters are frequently referred to as "shapers" since, in a time-domain view, they "shape" the response associated to the event. Filters can also be synthesized digitally, even though in most cases this is impractical due to constraints from power and real-estate budgets.

This contribution focuses on the design of low-noise analog shapers, but some basic blocks can be used as part of time-variant filters. The most frequently adopted shape is the semi-Gaussian, available in different orders (i.e. number of poles). Semi-Gaussian shapers are relatively easy to implement and can offer a signal-to-noise ratio within a few percent from the usually impractical optimal shapes. For example, assuming white series and white parallel noise contributions, the minimum Equivalent Noise Charge (ENC) for a high order semi-Gaussian shape is about 12.5% higher than the one for the optimum shape (i.e. infinite cusp) [2], [3].

Manuscript received April 14, 2011; revised July 18, 2011; accepted July 19, 2011. Date of publication August 30, 2011; date of current version October 12, 2011.

The authors are with the Instrumentation Division, Brookhaven National Laboratory, Upton, NY 11973 USA (e-mail: degeronimo@bnl.gov).

Color versions of one or more of the figures in this paper are available online at http://ieeexplore.ieee.org.

Digital Object Identifier 10.1109/TNS.2011.2162963

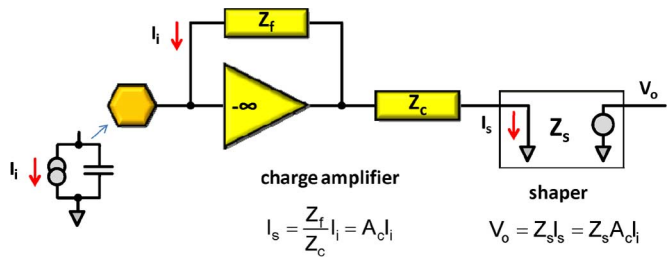

Fig. 1. First order schematic of a charge amplifier followed by a shaper.

In Section II we analyze the classical configurations based on voltage feedback with passive components. In Section III we briefly discuss some alternative configurations which make use of additional active devices in feedback to provide current scaling. Finally, in Section IV we introduce the concept of delayed dissipative feedback (DDF), which consists of delaying the resistive feedbacks from the furthest available nodes along the shaping chain. We will show that, in order to implement semi-Gaussian shapers, a small capacitor in positive feedback is required. The DDF technique can overcome some of the limitations of the more classical configurations. For example, in a third order shaper a factor of two higher dynamic range can be obtained or, at equal dynamic range, about 25% of the capacitance is needed (i.e. about 30% of the area in practical cases).

II. Noise and Dynamic Range in Classical Configurations

Charge amplifiers, along with providing low-noise amplification, offer a low input impedance (virtual ground) which stabilizes the potential of the sensor electrode and reduces the inter-electrode cross-talk. The charge amplifier is schematized in Fig. 1, where we assume an ideal voltage amplifier with infinite gain and bandwidth (a finite gain and bandwidth would have negligible consequence on our analysis—if the dc loop gain is high and the rise time is a small fraction of the peaking time).

The current I_i induced in the sensing electrode is amplified with current gain (or charge gain) A_c equal to the ratio of the feedback impedance Z_f and the coupling impedance Z_c. This ratio must be a real number (i.e. the gain A_c), in order to avoid undesired tails in the output current I_s injected in the next stage. The output current I_s is injected, with opposite polarity, into the next stage, which offers another virtual ground and represents the input stage of the shaper. The current (or charge) is then filtered and converted into a voltage V_o with transfer function Z_s. It is followed by further processing such as discrimination, peak- or time- detection, and/or counting. It is worth noting that the charge amplifier can be implemented using two or more charge-amplification stages with gains $A_{c1}, A_{c2}, \ldots$ and overall

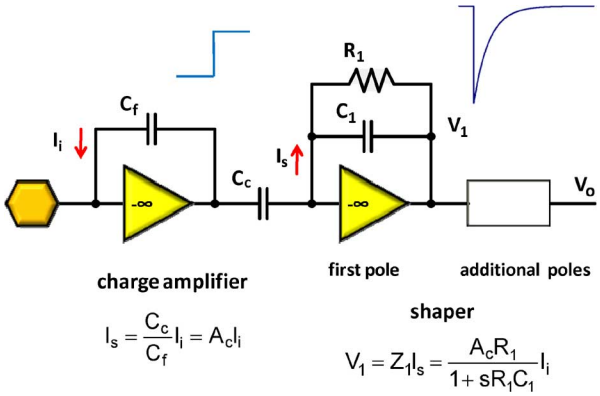

Fig. 2. Schematic of a charge amplifier assuming a capacitive feedback for the charge amplifier and a single-pole transimpedance amplifier as input stage of the shaper.

charge gain A_c given by the product of those. This is usually done when large values of A_c are required, such as for sensors generating very small signals.

For simplicity we assume for Z_f an infinite resistive component and a finite capacitive component C_f. This is justified considering that designers tend to keep the resistive component as high as possible in order to minimize the parallel noise contribution at the front-end. The coupling impedance will be capacitive according to $C_c = C_f A_c$. We also assume, initially, that the input stage of the shaper is realized using a transimpedance amplifier with feedback impedance $Z_1 = R_1//(1/sC_1)$, thus providing the first pole of the shaper with time constant $\tau_1 = R_1 C_1$. Finally, we assume that the shaper amplifiers are characterized by infinite gain and are noiseless. The latter is justified by the fact that, in most practical cases, the noise contribution from the amplifiers can be made negligible by increasing the size and power of the active devices (this is not always easy to achieve, and then the noise from the amplifier must be taken into account). The configuration resulting from these assumptions is shown in Fig. 2, where the output waveform V_1 in response to a charge Q is also shown, with peak amplitude $Q \cdot A_c/C_1$.

Starting from these assumptions and from the configuration in Fig. 2, we can calculate the contribution to the Equivalent Noise Charge (ENC) of the first stage of the shaper. The noise contribution comes from the dissipative component R_1 of the shaper [4]. The parallel noise spectral density of R_1 is given by $4\ kT/R_1$ and it can be reported as an equivalent parallel noise generator at the input of the charge amplifier by scaling it with the square of the charge gain A_c. It must be kept in mind that this is done for calculation purposes and the actual noise source is further down in the channel, not to be confused with the physical sources of parallel noise at the input. It follows the contribution to the ENC of R_1, given by:

$$ENC_{s1}^2 = \frac{a_p}{A_c^2}\frac{4kT}{R_1}\tau_p \qquad (1)$$

where a_p is the ENC coefficient for white parallel noise [2], [3], [5] and τ_p is the peaking time (from 1% to peak) of the shaped signal. It is worth noting that an analysis based on a front-end voltage amplifier without feedback (see for example Fig. 6.11 in [5]) would give A_c dependent on the input capacitance, which is not the case for the charge amplifier configuration in Fig. 2. From (1) it can be observed that the contribution decreases as A_c increases. Since the peaking time is proportional to the time constant, $\tau_p = \varepsilon_p R_1 C_1$, we can write:

$$ENC_{s1}^2 = \frac{a_p}{A_c^2}\frac{4kT}{R_1}\varepsilon_p R_1 C_1 = \frac{a_p \varepsilon_p}{A_c^2} 4kTC_1 \qquad (2)$$

where ε_p depends on the type of shaping. Table I summarizes the values of a_p and ε_p for semi-Gaussian shapers with real poles (even and odd) and complex conjugate poles (odd only) where the first stage gives the real pole. In Table I are also reported a_w (the ENC coefficient for white series noise) and the two coefficients χ (which takes into account the noise contribution of the next stages) and RDR (the relative dynamic range), both discussed later in this section.

TABLE I
COEFFICIENTS FOR UNIPOLAR SHAPERS WITH REAL (R) AND COMPLEX-CONJUGATE (C) POLES, DIFFERENT ORDERS

	RU-2	RU-3	RU-4	RU-5	RU-6	RU-7	CU-2	CU-3	CU-4	CU-5	CU-6	CU-7
a_w	0.92	0.82	0.85	0.89	0.92	0.94	0.93	0.85	0.91	0.96	1.01	1.04
a_p	0.92	0.66	0.57	0.52	0.48	0.46	0.88	0.61	0.51	0.46	0.42	0.40
ε_p	1	1.92	2.74	3.47	4.13	4.73	n/a	1.79	n/a	2.95	n/a	3.76
$a_p\,\varepsilon_p$	0.92	1.27	1.56	1.81	1.98	2.18	n/a	1.09	n/a	1.355	n/a	1.503
χ	1	1.13	1.24	1.31	1.37	1.43	n/a	5.5	n/a	5.5	n/a	5.5
RDR	1	0.82	0.72	0.66	0.62	0.59	n/a	0.51	n/a	0.45	n/a	0.43

It can now be observed that, for a given shaper, the contribution ENC_{s1} only depends on the values of A_c and C_1. The values of A_c and C_1 also define the maximum charge Q_{max} that the stage can process without saturation. If $V_{1\,max}$ is the maximum voltage swing at the output of the stage, it follows:

$$Q_{max}A_c = C_1 V_{1\,max} \quad \text{or} \quad A_c = \frac{C_1 V_{1\,max}}{Q_{max}}. \qquad (3)$$

We now express the dynamic range DR of the front-end as the ratio between the maximum charge Q_{max} and the total ENC, which includes the ENC_{ca} from the charge amplifier and the ENC_{s1} from the first stage of the shaper:

$$DR = \frac{Q_{max}}{\sqrt{ENC_{ca}^2 + ENC_{s1}^2}}. \qquad (4)$$

A design that aims at offering the highest possible resolution (lowest possible ENC) tends to keep ENC_{s1} negligible with respect to ENC_{ca}. Assuming about 10% (in power) it follows:

$$DR \approx \frac{Q_{max}}{\sqrt{11 \cdot ENC_{s1}^2}} = \frac{\frac{C_1 V_{max}}{A_c}}{\sqrt{11 \cdot \frac{a_p \varepsilon_p}{A_c^2} 4kTC_1}} = \frac{V_{1\,max}}{\sqrt{11 \cdot a_p \varepsilon_p \frac{4kT}{C_1}}}. \qquad (5)$$

It is important to observe that ENC_{ca} depends inherently on the input capacitance C_{IN} and on the peaking time τ_p. Here we assume that the charge amplifier has been already optimized for given C_{IN} and τ_p, and that the design of the shaper (with the 10% requirement on the contribution) follows from that. Equation (5) shows that the dynamic range increases with $V_{1\,max}$ and with the square root of C_1. For a given shaper and capacitor value C_1 the dynamic is maximized if $V_{1\,max} = V_{dd}$, where V_{dd} is the maximum voltage allowed by the technology, which means that the shaper amplifier must implement a rail-to-

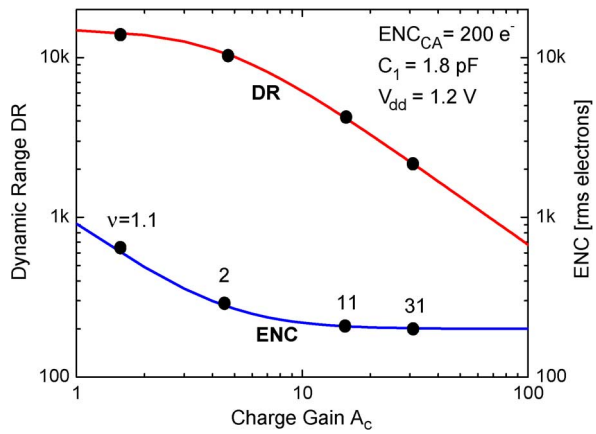

Fig. 3. Example of DR and ENC vs. charge gain Ac. The four cases of $\nu = 1.1$, 2, 11, and 31 are pointed out.

rail output stage. Further increase can only be achieved by increasing the value of C_1, which also means increasing A_c (as in (3)) and the area (and power) of the first stage of the shaper. For example, a CMOS 130 nm technology with 1.2 V supply and typical MIM capacitance of 2 fF/μm^2, assuming a CU-3 shaper ($a_p\varepsilon_p = 1.09$) with available area 30×30 μm, the dynamic range is limited, according to (5), to $DR < 3,600$.

For a given C_1, higher values of dynamic range can only be obtained at the expense of the ENC, and the maximum would be achieved when ENC_{s1} dominates over ENC_{ca}. Equation (5) can be written in the more general form:

$$DR = \frac{Q_{max}}{ENC_{ca}\sqrt{\frac{\nu}{\nu-1}}} \approx \frac{V_{dd}}{\sqrt{\nu \cdot a_p\varepsilon_p \frac{4kT}{C_1}}}$$

$$\nu = \frac{ENC^2}{ENC_{s1}^2} = \frac{ENC_{ca}^2 + ENC_{s1}^2}{ENC_{s1}^2} = 1 + \frac{ENC_{ca}^2}{ENC_{s1}^2}, \quad (6)$$

where $\nu > 1$ is the ratio between the squares of the total ENC and the ENC_{s1} from the first stage of the shaper: the higher the first stage contribution, the lower the value of ν.

Fig. 3 shows an example of compromise between ENC and dynamic range assuming the previous technology case and $ENC_{ca} = 200$ e$^-$. The four cases of $\nu = 1.1$, 2, 11, and 31 (corresponding to $(ENC_{ca}/ENC_{s1})^2 = 0.1$, 1, 10, and 30 respectively) are shown, and it can be observed how the dynamic range can be increased at the expense of the ENC. Values of ν lower than 1.1 (ENC dominated by ENC_{s1}) would not benefit much the DR but would further limit the resolution by increasing the total ENC. The extreme case is for $\nu = 1$ (i.e. no charge amplification) where $DR \approx 15,000$ and $ENC \approx 900$ e$^-$. On the other hand, values of ν higher than 11 (ENC dominated by ENC_{ca}) would not benefit much the ENC but would further limit the DR.

From (6) it is observed that a reduction in area at equal DR can be obtained by decreasing ν while keeping the ratio ν/C_1 constant (the charge gain A_c would decrease according to (3)). However, the ENC will increase according to the square root of $\nu/(\nu-1)$.

For practical cases, where ENC_{ca} and the maximum charge are given, a decrease in ν corresponds to a decrease in useful dynamic range according to the square root of $(\nu-1)/\nu$ (note

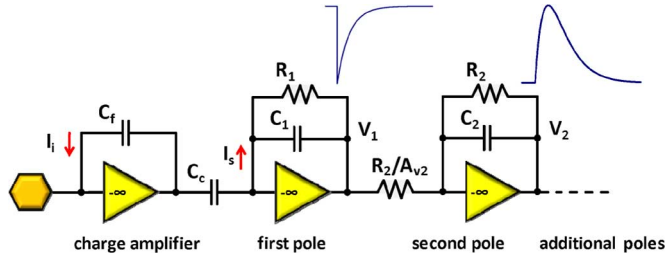

Fig. 4. Schematic of a charge amplifier followed by a shaper with real coincident poles.

that the maximum charge of interest may differ from the maximum charge Q_{max} that can be processed by the front-end). In other words, decreasing the value of ν increases the maximum charge beyond the one of interest, while still increases the value of ENC. In low-noise design, the increase in ENC is still acceptable if contained within $\sim$10% from ENC_{ca}, which means $\nu \geq 5.76$. For $\nu = 5.76$ the value of C_1 is reduced about 50% (factor 1.91) with respect to $\nu = 11$.

It is worth emphasizing one more time that, in this analysis, the ENC_{ca} is assumed defined and optimized for noise (i.e. the charge amplifier is designed for given C_{IN} and τ_p) and that the design of the shaper follows from that. From (6) it can also be observed that such defined DR does not depend on the peaking time τ_p. However, once the system is designed with a given optimized ENC_{ca} and a given ν, an adjustment of the peaking time (obtained scaling the value of the resistors) would in most cases change ENC_{ca} and then would modify ν and the DR (while the noise contribution from the shaper would not change).

So far we have assumed negligible the noise contribution from subsequent stages, which provide the additional poles of the shaper. We first consider the case of real coincident poles. These configurations are frequently referred to as "$CR-RC^{n-1}$ shapers" since they can be implemented using one CR filter followed by $n-1$ filters of RC type, and they are assumed to be connected at the voltage output of the charge amplifier. The resulting transfer function provides one zero in the origin, which compensates for the pole in the origin from the feedback capacitor of the charge amplifier, and n poles with time constant RC. The order of the shaper is equal to n (zeroes cancelled, n poles in total). The lowest possible order without divergence of noise is $n = 2$ (the well known and widely adopted CR-RC shaper). The equations in the frequency (Laplace) and time domains are as follows:

$$H(s) = \frac{1}{(s+p)^n}, \; h(t) = \frac{1}{(n-1)!}t^{n-1}\exp(-tp) \; n = 2, 3, 4, \ldots \quad (7)$$

where n is the order and p are the real poles, coincident.

Fig. 4 shows a frequently adopted configuration for $CR-RC^{n-1}$ shapers. Each additional i^{th} pole is obtained adding one stage with components C_i, R_i, and R_i/A_{vi}, where A_{vi} is the dc voltage gain. Assuming that the first stage operates rail-to-rail, as required to minimize its and the following noise contributions, the performance of the shaper is maximized when also the subsequent stages operate rail-to-rail, which is obtained with $A_{v2} \approx e$, $A_{v3} \approx e/2$, $A_{v4} \approx e/2.25$, $A_{v5} \approx e/2.36$, and so on. We can estimate the noise contribution of the two dissipative components of the second stage, i.e. R_2 and R_2/A_{v2}.

When reported as equivalent parallel generators at the input of the first pole, the noise spectral densities are respectively given by:

$$\begin{aligned} S_{R2} &= \frac{4kT}{R_2}\frac{R_2^2}{A_{v2}^2}\frac{1+\omega^2R_1^2C_1^2}{R_1^2} \\ &= \frac{4kT}{R_1}\frac{1}{A_{v2}^2}\frac{R_2}{R_1}\left(1+\omega^2R_1^2C_1^2\right) \\ S_{R2/Av2} &= 4kT\frac{R_2}{A_{v2}}\frac{1+\omega^2R_1^2C_1^2}{R_1^2} \\ &= \frac{4kT}{R_1}\frac{1}{A_{v2}}\frac{R_2}{R_1}\left(1+\omega^2R_1^2C_1^2\right) \end{aligned} \tag{8}$$

and they can be combined into a single noise generator:

$$S_2 = \frac{4kT}{R_1}\frac{C_1}{C_2}\frac{1}{A_{v2}}\left(1+\frac{1}{A_{v2}}\right)\left(1+\omega^2R_1^2C_1^2\right). \tag{9}$$

where we set $R_1C_1 = R_2C_2$ for coincident poles. Such contribution can be reported as an equivalent parallel noise generator at the input of the charge amplifier by scaling it with the square of the charge gain A_c. After a few steps it follows the contribution to the ENC of the second stage, given by:

$$\begin{aligned} ENC_{s2}^2 &= \frac{a_p\varepsilon_p}{A_c^2}4kTC_1\frac{C_1}{C_2}\frac{1}{A_{v2}}\left(1+\frac{1}{A_{v2}}\right)\left(1+\frac{a_w}{\varepsilon_p^2a_p}\right) \\ &= ENC_{s1}^2\frac{C_1}{C_2}\chi_2 \end{aligned} \tag{10}$$

where a_w is the ENC coefficient for white parallel noise and χ_2 depends on the order of the shaper with $\chi_2 \approx 1$ for the second order, 0.83 for the third order, 0.78 for the fourth order, and so on. From (10) it can be observed that the noise contribution from the second stage of the shaper, relative to the first, decreases as the order increases and as the C_2/C_1 ratio increases, and in principle can be made negligible for $C_2 \gg C_1$, i.e. at expenses of area and power.

As the order increases, the noise contribution from the next stages must be added. Eventually, the total contribution from the shaper can be written as:

$$ENC_s^2 = ENC_{s1}^2\left(1+\chi\frac{C_1}{C_s}\right), \tag{11}$$

where we assume rail-to-rail operation, C_s is the average capacitance per pole, and $\chi \approx 1$ for the second order, 1.13 for the third order, 1.24 for the fourth order, 1.3 for the fifth order, and so on. It is worth emphasizing that the contribution of each additional stage can be made negligible by increasing its capacitance relative to C_1, which at equal gain (rail-to-rail operation) corresponds to a reduction in the value of the resistors.

Next we consider the case of complex conjugate poles. These configurations, introduced by Ohkawa [6], have a number of advantages [7], among which a faster return to zero at equal peaking time with respect to the real poles of the same order. The equations in the frequency (Laplace) domain are:

$$\begin{aligned} H(s) &= \frac{1}{(s+p_1)\prod_{i=2}^{(n+1)/2}\left[(s+r_i)^2+i_i^2\right]} \quad n=3,5,7,\ldots \\ H(s) &= \frac{1}{\prod_{i=1}^{n/2}\left[(s+r_i)^2+i_i^2\right]} \quad n=2,4,6,\ldots \end{aligned} \tag{12}$$

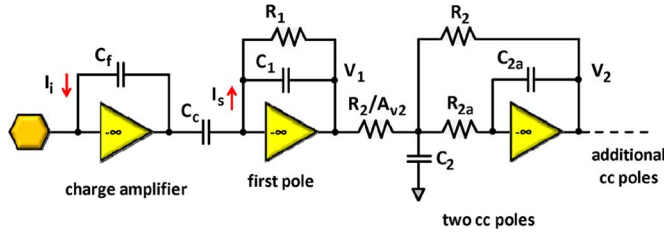

Fig. 5. Schematic of a charge amplifier followed by a shaper with complex conjugate poles.

where n is the order, p_1 is the real pole (n odd only), and r_j, i_j are the real and imaginary parts of the complex-conjugate poles, obtained as roots of the equation $(1/0!) - (s^2/1!) + (s^4/2!) - (s^6/3!) + \ldots (s^{2n}/n!) = 0$, while in the time domain are:

$$\begin{aligned} s(t) &= K_1\exp(-tp_1) + \sum_{i=2}^{(n+1)/2} 2|K_i|\exp(-tr_i)\cos(-ti_i+\angle K_i) \\ &\quad n=3,5,7,\ldots \\ s(t) &= \sum_{i=1}^{n/2} 2|K_i|\exp(-tr_i)\cos(-ti_i+\angle K_i) \\ &\quad n=2,4,6,\ldots \end{aligned} \tag{13}$$

where the coefficients K_i (magnitude $|K_i|$ and argument $\angle K_i$) are given by:

$$\begin{aligned} K_i &= \frac{1}{[-r_i-ji_i+p_1]\prod_{k=2,k\neq i}^{(n+1)/2}[-r_i-ji_i+r_k^2+i_k^2]-2ji_i} \\ &\quad i>1,\ n=3,5,7,\ldots \\ K_i &= \frac{1}{\prod_{k=1,k\neq i}^{n/2}[-r_i-ji_i+r_k^2+i_k^2]-2ji_i} \\ &\quad n=2,4,6,\ldots \end{aligned} \tag{14}$$

Fig. 5 shows a frequently adopted configuration for these shapers: if n is the order (odd in these cases), the real pole is given by the first stage and the complex conjugate poles are given by the $(n-1)/2$ additional stages. Each additional stage has transfer function:

$$\begin{aligned} H(s) &= -\frac{A_{vi}}{s^2R_iC_iR_{ia}C_{ia}+sC_i\left[R_i+R_{ia}(1+A_{vi})\right]+1} \\ &= \frac{A_{vi}}{\frac{s^2}{\omega_i^2}+\frac{s}{\omega_iQ_i}+1}, \end{aligned} \tag{15}$$

where the values of $\omega_0 = 1/\tau_0$ (real pole), ω_i and Q_i, normalized to the peaking time τ_p, can be obtained from Table II. The value of C_{ia} is about 20% of the value of C_i, and we can thus assume an average capacitance per pole $C_s \approx (C_i + C_{ia})/2$.

Evaluating the noise contribution of the dissipative components of these stages is cumbersome. Eventually, the total contribution from the shaper can be written again as in (11), where we assume again rail-to-rail operation, C_s is the average capacitance per pole, and $\chi \approx 5.5$ for all orders. In these configurations most of the noise contributions come from the series resistors R_{ia}. Once again it is worth emphasizing that, apart from the first stage (real pole), the contributions can be made negligible by increasing the value of the average capacitance per pole C_s.

TABLE II
DESIGN COEFFICIENTS FOR UNIPOLAR SHAPERS WITH COMPLEX-CONJUGATE POLES, DIFFERENT ORDERS

	$\omega_0\tau_p$	$\omega_1\tau_p$	Q_1	$\omega_2\tau_p$	Q_2	$\omega_3\tau_p$	Q_3
CU-2	-	1.031	0.541	-	-	-	-
CU-3	1.793	1.976	0.606	-	-	-	-
CU-4	-	2.471	0.514	2.812	0.672	-	-
CU-5	2.945	3.066	0.543	3.532	0.736	-	-
CU-6	-	3.400	0.507	3.612	0.576	4.178	0.797
CU-7	3.758	3.842	0.523	4.128	0.61	4.775	0.855

Table I summarizes the value of χ for various orders. Also included in Table I is the relative dynamic range RDR, i.e. the DR normalized to the one for the RU-2 case, assuming the same values for $\mathrm{ENC_{ca}}$ and ν (e.g. $\nu = 11$ which is the practical case where $\mathrm{ENC_s} = \mathrm{ENC_{ca}}/\sqrt{10}$), and assuming all shapers using the same value of $\mathrm{C_1}$ and $\mathrm{C_s} = \mathrm{C_1}$. From Table I it may appear that low order shapes offer a higher DR. A thorough comparative analysis, though, should include the impact of the shape on $\mathrm{ENC_{ca}}$. For example, under constraint of finite pulse width (e.g. rate constraint) and dominant white series noise, higher order shapes offer a lower $\mathrm{ENC_{ca}}$ due to the higher symmetry (i.e. longer peaking time at equal width). Higher order shapers can also offer some advantage in terms of pile-up reduction and ballistic deficit [7].

We conclude this section by applying these results to the (5) and (6) for the dynamic range, obtaining:

$$\mathrm{DR} \approx \frac{\mathrm{Q_{max}}}{\sqrt{\nu \cdot \mathrm{ENC_s^2}}} = \frac{\mathrm{V_{1\,max}}}{\sqrt{\nu \cdot \mathrm{a_p}\varepsilon_\mathrm{p} 4\mathrm{kT}\left(\frac{1}{\mathrm{C_1}} + \frac{\chi}{\mathrm{C_s}}\right)}}$$
$$\nu = \frac{\mathrm{ENC^2}}{\mathrm{ENC_{s1}^2}} = 1 + \frac{\mathrm{ENC_{ca}^2}}{\mathrm{ENC_{s1}^2}} \qquad (16)$$

For a given total capacitance $\mathrm{C_T} = \mathrm{C_1} + (\mathrm{n}-1)\mathrm{C_s}$, where n is the order of the shaper, the DR in (16) has a maximum around:

$$\mathrm{C_1} \approx \frac{\mathrm{C_T}}{1 + \sqrt{\chi(\mathrm{n}-1)}} \quad \mathrm{n} = \text{shaper order}, \qquad (17)$$

which, for all of low order shapers and the high order shapers with complex conjugate poles, is about $\mathrm{C_T/n}$ while for high order shapers with real coincident poles is somewhat lower. The rest of the capacitance can be distributed in equal amount among the additional poles, but it should be observed that slightly better results can be obtained assigning larger capacitance values to the last stages. Since the maximum is relatively shallow, the value of DR obtained for $\mathrm{C_T/n}$ is still a good approximation.

In the previously reported example with $\mathrm{C_s} = \mathrm{C_1} = 1.8\ \mathrm{pF}$, $\mathrm{ENC_{ca}} = 200\ \mathrm{e^-}$, $\nu = 11$ it follows $\mathrm{DR} < 1,400$ and 2,800 for CU-3 and RU-2 respectively. With the described configurations and assuming comparable area and power and given $\mathrm{ENC_{ca}}$, the shapers with real poles offer a dynamic range about 70% higher than the ones with complex conjugate poles.

III. ALTERNATIVE CONFIGURATIONS

In this Section we review some configurations which can be found, in part, in the literature and that could provide an alternative solution to the voltage feedback circuit for realizing low-noise single pole stages. The review would like to provide insights on performance and noise analysis, without aiming at being exhaustive. Some valuable information can also be found in [8], [9].

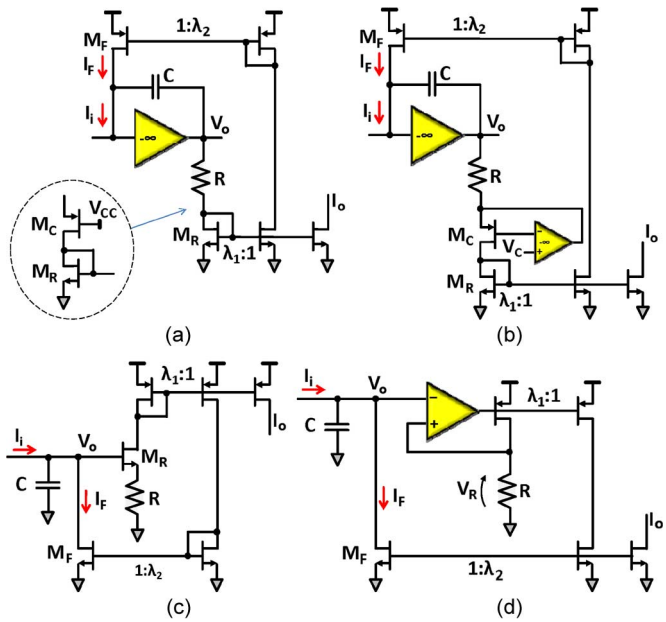

Fig. 6. Alternative configurations for the realization of low-noise single-pole stages.

The alternative configurations are shown in Fig. 6. They make use of CMOS current mirrors to scale down the current in the resistor R, thus reducing its noise contribution. In fact, if $\lambda = \lambda_1\lambda_2$ is the scaling factor, the dissipative current feedback $\mathrm{I_F}$ through $\mathrm{M_F}$ can be approximated as $\mathrm{I_F} \approx \mathrm{V_o/R_{eq}}$, where $\mathrm{R_{eq}} = \mathrm{R}\cdot\lambda$. is the equivalent resistance which sets, with C, the time constant of the filter, given by $\mathrm{C}\cdot\mathrm{R_{eq}}$. The parallel noise contribution from R, reported at the input of the stage, scales down with λ^2, being given by $4\,\mathrm{kT}/(\mathrm{R}\cdot\lambda^2)$, i.e. $4\,\mathrm{kT}/(\mathrm{R_{eq}}\cdot\lambda)$. It results that, at equal C and time constant, the noise contribution from R is a factor λ lower than the one from $\mathrm{R_1}$ in the corresponding configuration of Fig. 2.

On the other hand, design constraints for linearity and dynamic range suggest that the dominant noise contribution comes from the channel noise of the last transistor of the feedback chain, $\mathrm{M_F}$.

We start analyzing the configuration in Fig. 6(a). This configuration can also make use of a cascode stage $\mathrm{M_C}$, as shown in the detail in Fig. 6(a), frequently used in complementary configurations [10], [11]. In order to guarantee a linear response, the relationship $\mathrm{R}\cdot\mathrm{g_{mR}} \gg 1$ must be satisfied, where $\mathrm{g_{mR}}$ is the transconductance of $\mathrm{M_R}$ (or the one of the cascode MOSFET, if applicable). This relationship imposes a limit to the minimum current $\mathrm{I_R}$ flowing through R. Assuming that $\mathrm{M_R}$ operates in moderate inversion (as required to mirrors to guarantee a large enough voltage swing), its $\mathrm{g_m}$ can be approximated as $\mathrm{g_{mR}} \approx \mathrm{I_R/nV_T}$, where n is the sub-threshold factor ($\mathrm{n} \approx 1.2$ typical) and $\mathrm{V_T} = \mathrm{kT/q}$ is the thermal voltage (~25 mV at 300 K). It follows the requirement on the voltage drop across R, given by $\mathrm{R}\cdot\mathrm{I_R} \gg \mathrm{nV_T}$. Since $\mathrm{M_F}$ operates in moderate inversion, its

white noise spectral density is given by $S_{nMF} = 2qI_F$. By considering the mirror ratio and by imposing the relationship for linear response it follows:

$$S_{nMF} = 2qI_F = \frac{2qI_R}{\lambda} \gg \frac{2qnV_T}{R\lambda} = \frac{2kT}{R_{eq}}, \qquad (18)$$

which shows that, at equal C and time constant (i.e. when $R_{eq} = R_1$) the noise spectral density from M_F would dominate, and it would be larger than the one from R_1 in Fig. 2, given by 4 kT/R_1. The low-frequency noise component from M_F should also be added, but this contribution can be reduced, to some extent, by increasing the gate area of M_F (i.e. by increasing both L and W of M_F). Finally, the non-stationary noise contribution [12] should be considered, associated to the increase in the drain current of M_F in presence of a signal. In the time domain this contribution, integrated in C, can be approximated as $qi_F\tau_P/C^2$ where i_F is the signal current and τ_P is the peaking time (a measure of the integration time). On the other hand, the signal integrated in C is given by QA_c/C, where Q is the input charge and A_c is the charge amplifier gain. By considering that $i_F\tau_P \approx QA_c$ it follows for the signal-to-noise ratio due to the non-stationary contribution:

$$\left(\frac{S}{N}\right)_{ns} \approx \frac{QA_c}{C}\sqrt{\frac{C^2}{qQA_c}} = \sqrt{\frac{Q}{q}A_c} = \sqrt{NA_c}, \qquad (19)$$

where N is the number of signal electrons at the input of the charge amplifier. In most practical cases this contributions has negligible impact on the total S/N due to $A_c \gg 1$, as it can be observed assuming a minimum signal $N \approx ENC$ (ENC in number of electrons).

Attempts to improve the linearity by controlling the gate voltage of the cascode M_C can be considered, as shown in Fig. 6(b) and in [13]. However, the noise contribution from the controlling stages must be taken into account; also, maintaining the voltage drop across R below the thermal voltage V_T might be a challenge.

Most of the previous arguments also apply to the configuration in Fig. 6(c) [14], where the M_R is now the MOSFET used as source follower.

With regards to the configuration in Fig. 6(d), ideally the voltage drop across R_1 can be kept small but, in practical cases, it is difficult to reduce it to values much lower than the thermal voltage V_T, and (18) would still apply.

A further challenge towards the various configurations in Fig. 6 is to obtain a high linearity in the mirror stages over a wide dynamic range of currents. On the positive side, these configurations, at equal capacitance, use resistors of lower value thus reducing the relative area, even though the additional area for the current mirrors should now be accounted for.

These observations suggest that the linear configurations that make use of active devices in the signal path (e.g. current mirrors) cannot offer a dynamic range wider than the ones based on passive components only. It should be observed that OTA-based CMOS stages would enter this category as well [15]. The use of BiCMOS technologies would greatly alleviate the limitation in linearity, as shown in [16], but some of the limitations previously discussed still apply, including the loss due to the voltage drops. The same reference, interestingly, moves in the direction of delaying the feedback, which can offer improvements in noise. In the next section we introduce the concept of delayed dissipative feedback (DDF), applied to voltage-based configuration.

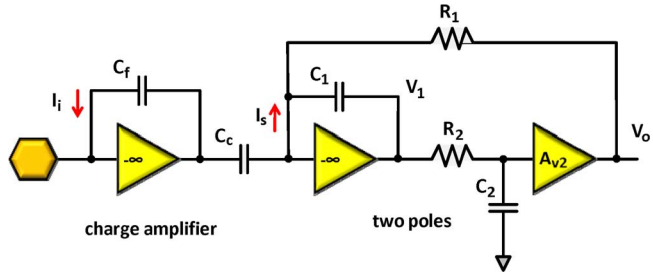

Fig. 7. Delayed dissipative feedback (DDF) applied to a second order shaper.

IV. A Lower-Noise Configuration: The Delayed Dissipative Feedback (DDF)

In this section we discuss configurations that perform beyond the DR limits imposed by (16). The approach consists of delaying wherever possible the feedback of the resistive (dissipative) components. An example of this concept, applied to a second order filter, is shown in Fig. 7.

In this configuration the resistive (dissipative) feedback to the input of the shaper is provided through R_1 from the output V_o, which is delayed by the time constant R_2C_2 and amplified, rather than from V_1.[1] Note that A_{v2} must be positive in order for the feedback through R_1 to be negative. The input stage of the amplifier A_{v2} is not a virtual ground, but does not need to be rail-to-tail. The transfer function V_o/V_1 can be alternatively implemented using an active filter, with minor impact on the noise performance.

The transfer function can be easily calculated as:

$$\frac{V_o}{I_s} = \frac{R_1}{s^2\frac{R_1C_1R_2C_2}{A_{v2}} + s\frac{R_1C_1}{A_{v2}} + 1}. \qquad (20)$$

It can be verified that two real and coincident poles with time constant τ_o are obtained if $R_1C_1 = 2\tau_oA_{v2}$ and $R_2C_2 = \tau_o/2$. Assuming that the first stage operates rail-to-rail, the performance of the shaper is maximized when also the next stage operates rail-to-rail, which is obtained for $\varepsilon_p = \tau_o/R_1C_1 = 1/e$ (i.e. the ratio between the peaking time and R_1C_1 is a factor ~2.718 lower than the case in Fig. 3). It also follows the value of $A_{v2} = e/2$. We can now calculate the noise contribution of the two dissipative components, R_1 and R_2. Concerning R_1, the result in (2) still applies, where $a_p = 0.92$ (from Table I). The contribution from R_2 can be either calculated or simulated. The total contribution from the shaper can be written as in (11) with $\chi \approx 1.35$ and the dynamic range as in (16) with a maximum, again, for $C_2 \approx C_1$. When compared with the same order configuration in Fig. 4, the noise power of this configuration at equal total capacitance is less than a half ($a \sim 0.44$ factor) and the dynamic range is about 50% higher ($a \sim 1.52$ factor).

[1]This specific configuration, limited to $A_{v2} = 1$, has been first envisioned by F. S. Goulding [17] and then widely adopted.

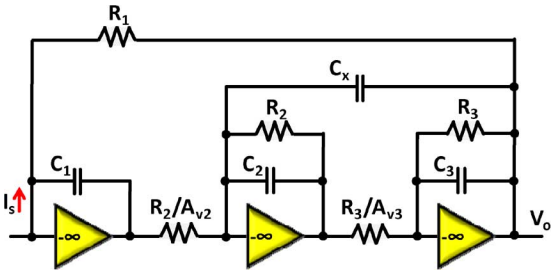

Fig. 8. Delayed dissipative feedback (DDF) applied to a third order shaper.

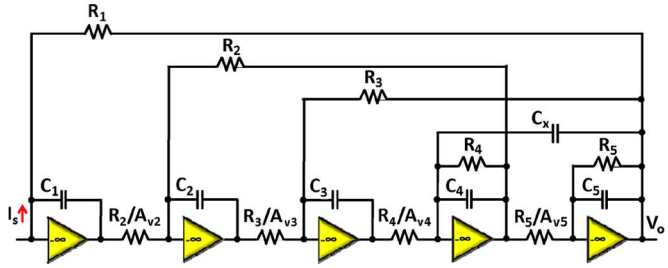

Fig. 9. Delayed dissipative feedback (DDF) applied to a fifth order shaper.

The configuration in Fig. 7 can also be used to realize a second order shaper with two complex conjugate poles. This is obtained for $R_1C_1 = A_{v2}/(\omega_1 Q_1)$ and $R_2C_2 = Q_1/\omega_1$ where the values of ω_1 and Q_1 can be obtained from Table II. For this configuration the values of ε_p and χ are 0.4 and 1.38 respectively. The noise power at equal capacitance and the dynamic range are comparable to the ones for the previous case of real poles, with the advantage of a slightly faster return to baseline at equal peaking time.

The delayed dissipative feedback can be used for higher order configurations as well. Fig. 8 show an example of a third order realization, which has transfer function:

$$\frac{V_o}{I_s} = \frac{R_1}{s^3\frac{\tau_1\tau_2\tau_3}{A_{v2}A_{v3}} + s^2\frac{\tau_1[\tau_2(1-\alpha_x)+\tau_3]}{A_{v2}A_{v3}} + s\frac{\tau_1}{A_{v2}A_{v3}} + 1}. \quad (21)$$

where $\tau_1 = R_1C_1$, $\tau_2 = R_2C_2$, $\tau_3 = R_3C_3$, and $\alpha_x = A_{v3}\tau_{2x}/\tau_2$ (here $\tau_{2x} = R_2C_x$). It is important to observe that without the small capacitance C_x in positive feedback it would not be possible to obtain a semi-Gaussian shaper, either with real coincident or with complex conjugate poles. In the case of real coincident poles with time constant τ_o, it follows:

$$\frac{\tau_1\tau_2\tau_3}{A_{v2}A_{v3}} = \tau_o^3,\ \frac{\tau_1[\tau_2(1-\alpha_x)+\tau_3]}{A_{v2}A_{v3}} = 3\tau_o^2,\ \frac{\tau_1}{A_{v2}A_{v3}} = 3\tau_o. \quad (22)$$

which, once solved, yields:

$$A_{v2} = \frac{\tau_1}{3\tau_o A_{v3}},\ \tau_2 = \frac{1}{2}\frac{\tau_o}{1-\alpha_x}\left(1 \pm \sqrt{1-\frac{4}{3}(1-\alpha_x)}\right),\ \tau_3 = \frac{\tau_o^2}{3\tau_2}. \quad (23)$$

The values $\varepsilon_p = 0.52$ and $A_{v3} = 1.08$ should be chosen in order to have all stages operating at equal output voltage range (i.e. rail-to-rail), which also corresponds to the minimum noise at equal gain. Finally, the condition $\alpha_x \geq 0.25$ must be satisfied, where $\alpha_x = 0.25$ ($C_x \approx C_2/4$) offers the minimum noise. The consequent value of χ to be used in (11) is 3.6. When compared to the same order configuration in Fig. 4, the noise power at equal total capacitance is a factor 0.58 lower and the dynamic range is about 31% higher.

The configuration in Fig. 8 can also be used to realize a third order shaper with complex conjugate poles, by imposing:

$$\begin{aligned} \frac{\tau_1\tau_2\tau_3}{A_{v2}A_{v3}} &= \frac{1}{\omega_0\omega_1^2}, \\ \frac{\tau_1[\tau_2(1-\alpha_x)+\tau_3]}{A_{v2}A_{v3}} &= \frac{1}{\omega_0\omega_1 Q_1} + \frac{1}{\omega_1^2}, \\ \frac{\tau_1}{A_{v2}A_{v3}} &= \frac{1}{\omega_0} + \frac{1}{\omega_1 Q_1}. \end{aligned} \quad (24)$$

TABLE III
COEFFICIENTS FOR DDF SHAPERS

	RU-2^{DDF}	RU-3^{DDF}	RU-5^{DDF}	CU-2^{DDF}	CU-3^{DDF}	CU-5^{DDF}
ε_p	0.368	0.52	0.67	0.4	0.57	0.81
χ	1.35	3.6	11.7	1.38	4.32	13.8
RDR_{DDF}	1.52	1.08	0.66	1.48	1	0.58
RDR_{DDF}/RDR	1.52	1.32	1	-	1.96	1.3

The values $\varepsilon_p = 0.57$ and $A_{v3} = 1.08$ should be chosen in order to have all stages operating at rail-to-rail output, which also corresponds to the minimum noise at equal gain. The condition $\alpha_x \geq 0.35$ must be satisfied, where $\alpha_x = 0.35$($C_x \approx C_2/3$) offers the minimum noise. The consequent value of χ to be used in (11) is 4.32. When compared to the same order configuration in Fig. 5, the noise power at equal total capacitance is a factor 0.26 lower and the dynamic range is about 95% higher.

Finally, Fig. 9 show an example of a fifth order realization. Also this configuration can be used for real or complex conjugate poles. The transfer function can be written as:

$$\begin{aligned} \frac{V_o}{I_s} = R_1 \cdot \Bigg\{ & s^5\frac{\tau_1\tau_2\tau_3\tau_4\tau_5}{A_{v2}A_{v3}A_{v4}A_{v5}} + s^4\frac{\tau_1\tau_2\tau_3[\tau_4(1-\alpha_x)+\tau_5]}{A_{v2}A_{v3}A_{v4}A_{v5}} \\ & + s^3\frac{\tau_1\tau_2\tau_3}{A_{v2}A_{v3}A_{v4}A_{v5}} + s^2\left(\frac{\tau_1\tau_5}{A_{v2}A_{v5}} + \frac{\tau_1\tau_2}{A_{v2}A_{v3}}\right) \\ & + s\frac{\tau_1}{A_{v2}A_{v5}} + 1\Bigg\}^{-1} \end{aligned} \quad (25)$$

where $\tau_1 = R_1C_1$, $\tau_2 = R_2C_2$, $\tau_3 = R_3C_3$, $\tau_4 = R_4C_4$, $\tau_5 = R_5C_5$, and $\alpha_x = A_{v4}\tau_{4x}/\tau_4$ (here $\tau_{4x} = R_4C_x$).

Table III summarizes the coefficients and performance achievable using the delayed dissipative feedback (DDF). The RDR_{DDF} is relative to the RU-2 case in Table I.

A comparison between Table I and Table III shows that the DDF is particularly beneficial with the low and medium medium order shapers. This is also highlighted observing the ratio RDR_{DDF}/RDR in Table III. A very promising configuration seems to be $CU-3^{DDF}$ where a factor of two higher dynamic range can be achieved with respect to the classical configuration. With high order cases the impact is small or negligible due to the noise contribution from the additional poles (see increase in coefficient χ). However, the use of larger values for R_1 reduces in all cases the value of the current required to generate the dc voltage drops, thus reducing its noise contribution. It is worth emphasizing, again, that a thorough

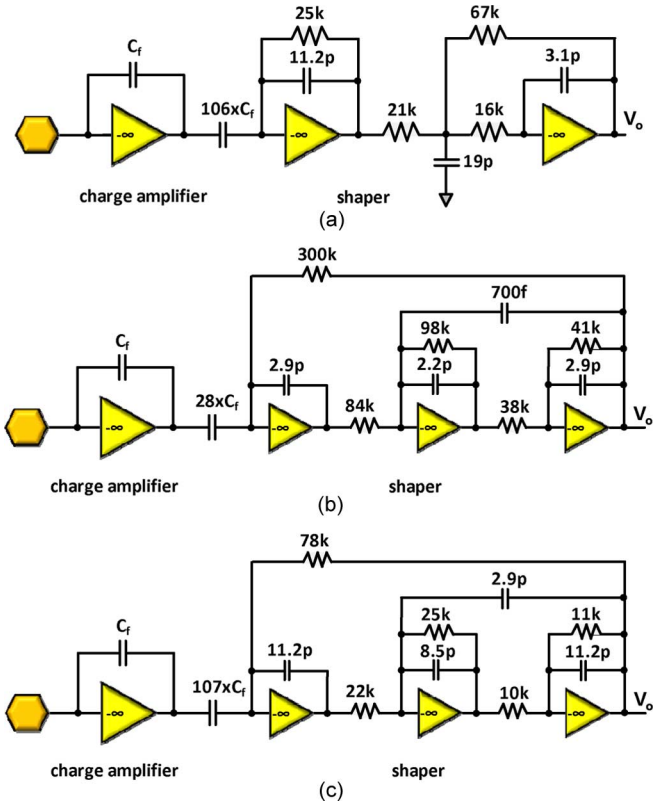

Fig. 10. Examples of realizations using the approach in Fig. 5 (a) and the DDF in Fig. 8 at equal dynamic range (b) and at equal total capacitance (c).

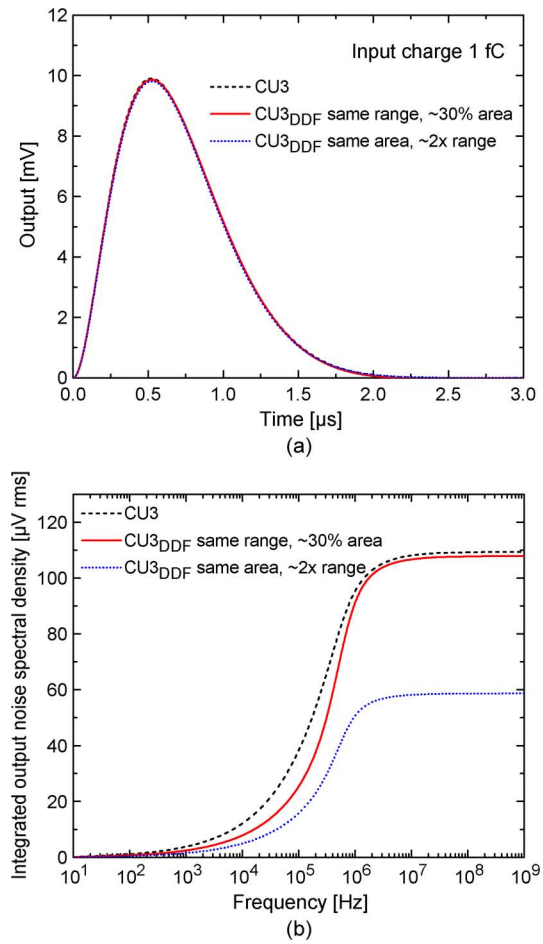

Fig. 11. Simulated pulse response (a) and integrated output noise spectral density (a) for the circuits in Fig. 10.

comparative analysis should include the impact of the shape on $\mathrm{ENC_{ca}}$ [7].

As a design example, let's consider the case of a CdZnTe based Gamma-ray detection system which must operate in the 10 keV to 3 MeV range with an electronic resolution better than 1 keV FWHM (e.g. ENC $\approx$ 90 electrons rms). In a first phase we design and optimize the charge amplifier in order to meet the required resolution. In doing so we assume a third order a semi-Gaussian shaper with complex conjugate poles and select a peaking time of 500 ns.

The design of the shaper starts from the requirements on the dynamic range and resolution. We would like to keep negligible the noise contribution from the shaper, hence selecting $\nu \geq 11$ in (16). It follows from (16), Table I, and a CMOS 130 nm technology (1.2 V and MIM capacitance 2 fF/μm^2)

$$\frac{3\ \mathrm{MeV}}{1\ \mathrm{keV}} = 3 \cdot 10^3 \leq \frac{1}{\sqrt{6.7\varepsilon_p 4\mathrm{kT}\left(\frac{1+\chi}{\mathrm{C}}\right)}}$$

$$\text{or} \quad \mathrm{C} \geq 6 \cdot 10^7 \varepsilon_\mathrm{p} 4\mathrm{kT}(1+\chi) \approx 960\ \mathrm{fF}\varepsilon_p(1+\chi) \quad (26)$$

where C is the average capacitance per pole, and we considered room temperature and a linear operation up to about 100 mV from the rails (i.e. 1 V maximum swing).

If we design the shaper using the configuration in Fig. 5, where $\varepsilon_\mathrm{p} \approx 1.79$ and $\chi \approx 5.5$, we get for the total shaper capacitance $\mathrm{C_{tot}} \geq 33.5$ pF, which corresponds to a minimum area of about 16,750 μm^2 (e.g. $\sim 130\ \mu\mathrm{m} \times 130\ \mu\mathrm{m}$). If we design using the configuration in Fig. 8, where $\varepsilon_\mathrm{p} \approx 0.57$ and $\chi \approx 4.32$, we get for the total shaper capacitance $\mathrm{C_{tot}} \geq 8.7$ pF, which corresponds to a minimum area of about 4,365 μm^2 (e.g. $\sim 66\ \mu\mathrm{m} \times 66\ \mu\mathrm{m}$). The required total resistance is ~ 130 kΩ in the first case and ~ 560 kΩ in the second case. The corresponding area in the selected technology for linear resistors, characterized by $\sim 350\ \Omega/\mathrm{square}$, is in minimum size about 70 μm^2 and 270 μm^2 respectively. Once we include the relatively small area for amplifiers and routings, the first case requires at least 18,000 μm^2 (e.g. about $135\ \mu\mathrm{m} \times 135\ \mu\mathrm{m}$) while the second 5,000 μm^2 (e.g. $71\ \mu\mathrm{m} \times 71\ \mu\mathrm{m}$), with a saving in area of about 72%. Additionally, the value of charge gain $\mathrm{A_c}$ is $\sim$107 in the first case and $\sim$28 in the second case, and the current needed to generate the dc voltage drops is more than 10 times lower.

In Fig. 10 the realization of the first (a) and second (b) case are shown, along with a third case where we use again the DDF, but with a total capacitance equal to the one of the first case. In Fig. 11 the simulations of the pulse response to 1 fC (a) and the integral of the output noise power spectral density (b) for all three cases are shown. It can be observed that, compared to the first case (a), the second (b) has comparable noise with a capacitance about four times lower (a saving in area of about 70%) while the third case (c) has about half of the rms noise at comparable total capacitance. In this simulation the noise contributions from the amplifiers are not included for the previously given reasons. To a first order, the noise contribution from the first amplifier of the shaper depends only on the value of $\mathrm{C_f}$ thus being comparable in all three cases.

V. Conclusions

Our analysis on the design of low-noise linear shapers suggests that, once the ENC from the charge amplifier is defined, the dynamic range of the system is set by the voltage swing and the value of the capacitance realizing the poles of the shaper, independent of the peaking time. The configuration used to realize the pole(s) has also relevant impact. Those configurations based on passive components in feedback offer a better dynamic range than the ones based on both active and passive components, as for scaling mirrors. The delayed dissipative feedback (DDF) can overcome some of the limitations of the more classical configurations. The DDF consists of delaying the resistive feedbacks from the furthest available nodes along the shaping chain. In order to implement semi-Gaussian shapers, a small capacitor in positive feedback is required. As an example, for a third order shaper a factor of two higher dynamic range can be obtained with the DDF or, at equal dynamic range, about 25% of the capacitance is required by the DDF (i.e. about 30% of the area in practical cases).

Acknowledgment

The authors are very grateful to Veljko Radeka and Pier Francesco Manfredi for stimulating discussions, and to Venetios Polychronakos for his encouragement and support. The authors are also grateful to the reviewers, editor, and senior editor for the valuable feedback.

References

[1] G. F. Knoll, *Radiation Detection and Measurement*, 3rd ed. New York: Wiley, 2000.

[2] V. Radeka, "Low noise techniques in detectors," *Ann. Rev. Nucl. Part. Sci.*, vol. 38, pp. 217–277, 1988.

[3] E. Gatti and P. F. Manfredi, "Processing the signals from solid state detectors in elementary particle physics," *La Rivista del Nuovo Cimento*, vol. 9, pp. 1–147, 1986.

[4] A. F. Arbel, "The second stage noise contribution of a nuclear pulse amplifier," *IEEE Trans. Nucl. Sci.*, vol. NS-15, no. 5, pp. 2–5, Oct. 1968.

[5] V. Radeka, "Signal processing for particle detectors," H. Schopper, Ed. , Landolt-Bornstein ser. New Series I/21B1, in press.

[6] A. Ohkawa, M. Yoshizawa, and K. Husimi, "Direct synthesis of the Gaussian filter for nuclear pulse amplifiers," *Nucl. Instrum. Methods*, vol. 138, pp. 85–92, 1979.

[7] G. De Geronimo, A. Dragone, J. Grosholz, P. O'Connor, and E. Vernon, "ASIC with multiple energy discrimination for high rate photon counting applications," *IEEE Trans. Nucl. Sci.*, vol. 54, no. 2, pp. 303–312, Apr. 2007.

[8] R. Schaumann and M. E. van Valkenburg, *Design of Analog Filters*. New York: Oxford Univ. Press, 2001.

[9] T. Deliyannis, Y. Sun, and J. K. Fidler, *Continuous-Time Active Filter Design*. Boca Raton, FL: CRC Press, 1999.

[10] R. L. Chase, A. Hrisoho, and J. P. Richer, "8-channel CMOS preamplifier and shaper with adjustable peaking time and automatic pole-zero cancellation," *Nucl. Instrum. Methods Phys. Res. A*, vol. 409, pp. 328–331, 1998.

[11] C. Fiorini and M. Porro, "Integrated RC cell for time-invariant shaping amplifiers," *IEEE Trans. Nucl. Sci.*, vol. 51, no. 5, pp. 1953–1960, Oct. 2004.

[12] G. De Geronimo and P. O'Connor, "A CMOS detector leakage current self adaptable continuous reset system: Theoretical analysis," *Nucl. Instrum. Methods Phys. Res. A*, vol. 421, pp. 322–333, 1999.

[13] I. I. Jung, J. H. Lee, C. S. Lee, and Y. W. Choi, "Design of high-linear CMOS circuit using a constant transconductance method for gamma-ray spectroscopy system," *Nucl. Instrum. Methods Phys. Res. A*, vol. 629, pp. 277–281, 2001.

[14] G. Bertuccio, P. Gallina, and M. Sampietro, "'R-Lens filter': An $(RC)^n$ current-mode low-pass filter," *IEEE Electron. Lett.*, vol. 35, no. 15, pp. 1209–1210, 1999.

[15] T. Noulis, C. Deradonis, S. Siskos, and G. Sarrabayrouse, *Nucl. Instrum. Methods Phys. Res. A*, vol. 583, pp. 469–478, 2007.

[16] S. Buzzetti and C. Guazzoni, "A novel compact topology for high-resolution CMOS/BiCMOS spectroscopy amplifiers," *IEEE Trans. Nucl. Sci.*, vol. 52, no. 5, pp. 1611–1616, Oct. 2005.

[17] F. S. Goulding, D. A. Landis, and N. Madden, "GAMMASPHERE—Elimination of ballistic deficit by using a quasi-trapezoidal pulse shaper," *IEEE Trans. Nucl. Sci.*, vol. 41, no. 4, pp. 1140–1143, Aug. 1994.